

Feedback from Tissue Mechanics Self-Organizes Efficient Outgrowth of Plant Organ

Jason Khadka,¹ Jean-Daniel Julien,¹ and Karen Alim^{1,2,*}

¹Max Planck Institute for Dynamics and Self-Organization, Göttingen, Germany and ²Physik Department, Technical University of Munich, Munich, Germany

ABSTRACT Plant organ outgrowth superficially appears like the continuous mechanical deformation of a sheet of cells. Yet, how precisely cells as individual mechanical entities can act to morph a tissue reliably and efficiently into three dimensions during outgrowth is still puzzling, especially when cells are tightly connected as in plant tissue. In plants, the mechanics of cells within a tissue is particularly well-defined because individual cell growth is essentially the mechanical yielding of the cell wall in response to internal turgor pressure. Cell-wall stiffness is controlled by biological signaling, which is impacted by stresses, and hence, cell growth is observed to respond to mechanical stresses building up within a tissue. What is the role of the mechanical feedback during morphing of tissue in three dimensions? Here, we develop a three-dimensional vertex model to investigate tissue mechanics at the onset of organ outgrowth at the tip of a plant shoot. We find that organ height is primarily governed by the ratio of growth rates of faster-growing cells initiating the organ versus slower-growing cells surrounding them. Remarkably, the outgrowth rate is higher when cell growth responds to the tissue-wide mechanical stresses. Our quantitative analysis of simulation data shows that tissue mechanical feedback on cell growth can act via a twofold mechanism. First, the feedback guides patterns of cellular growth. Second, the feedback modifies the stress patterns on the cells, consequently amplifying and propagating growth anisotropies. This mechanism may allow plants to grow organs efficiently out of the meristem by reorganizing the cellular growth rather than inflating growth rates.

SIGNIFICANCE All areal organs in plants begin as outgrowth from the shoot apical meristem. Organs are initiated by a rapidly expanding patch of cells on the shoot apical meristem surface. Yet, it is unclear how quicker cell growth can generate outgrowth, given that cells are tightly connected by shared cell walls within the tissue. Here, we build a three-dimensional vertex model of tissue growth. In particular, we account for mechanical feedback of tissue-wide stresses on cell growth. We find that the mechanical feedback is pivotal for efficient outgrowth because it self-organizes anisotropic growth of outgrowth boundary cells, allowing the primordia to bulge out. This mechanism allows for self-organized differentiation of cell growth patterns, likely relevant well beyond the model system studied here.

INTRODUCTION

Stochastic cellular growth and division result in robust and reproducible shaped tissues and organisms. What leads to this robustness on a tissue-wide scale, despite the apparent stochasticity on the cell scale, has been a puzzling question in biology (1–4). In plants, cells are enclosed by rigid cell walls, and the mechanics of these walls dictates cell growth. Anisotropic stiffness of the walls leads to anisotropic growth of cells (5). Most strikingly, the growth of cells is coupled

mechanically through shared walls. Expansion of one cell is communicated to all immediate neighbors through forces on cell walls and junctions. This mechanical coupling, along with biochemical signaling, has been proposed as the organizer of growth (6–8). However, a theoretical framework for studying the role of mechanics in dynamically morphing tissues in three dimensions is still missing to elucidate how a tissue can self-organize its shape.

Cell growth in plants largely results from yielding of the cell wall under internal turgor pressure (9,10). The directional yielding of cell walls due to their anisotropic properties is behind the anisotropic growth of the plant cells. It has been long observed that cellulose microfibrils of the cell wall are oriented in a transverse direction in elongating cells (11). The microfibrils, which are bound together by

Submitted February 12, 2019, and accepted for publication October 15, 2019.

*Correspondence: k.alim@tum.de

Editor: Lisa Manning.

<https://doi.org/10.1016/j.bpj.2019.10.019>

© 2019 Biophysical Society.



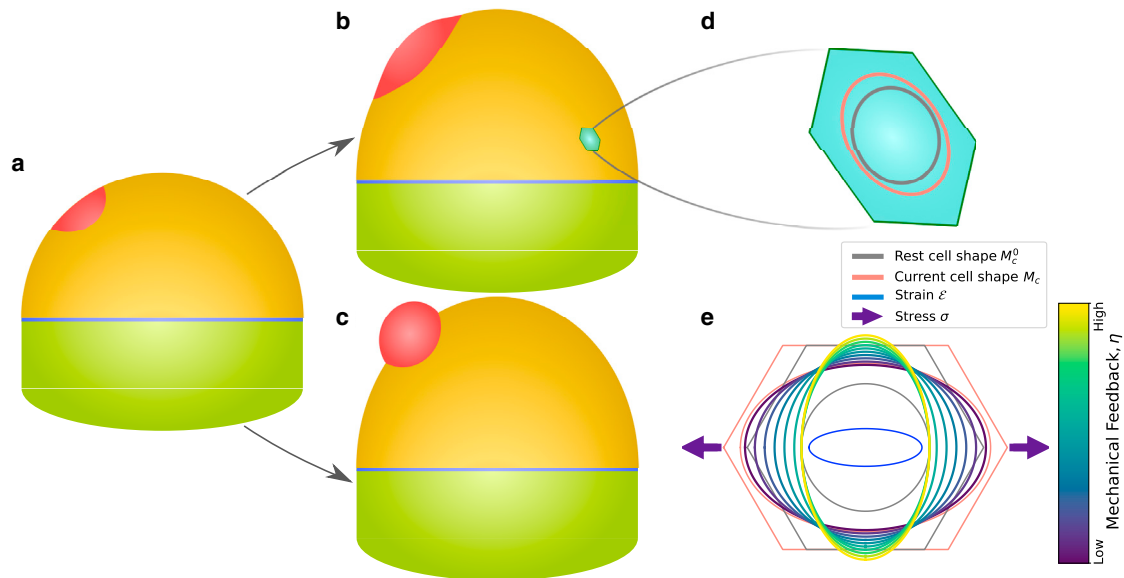


FIGURE 1 The outgrowth of aerial organs in plants starts from primordia on the shoot apical meristem (SAM). (a)–(c) show the growth of primordia from a group of faster-growing cells (red) on the SAM. (a) The SAM (yellow) is taken to be initially shaped like a dome. The red patch on the SAM shows the region of incipient primordium. The vertices at the boundary of SAM (blue line) are taken to be fixed because they are connected to hardened shoot (green base). The faster growth of primordia cells can either spread out on the surface of SAM, shown in (b), or it can bulge out of the SAM like in (c), laying the foundation for organogenesis. (d) The polygonal cells that make up the SAM dome for the simulation are defined by two key shape matrices. The rest cell shape matrix M_c^0 (gray ellipse) is the rest shape of the cell that it would attain without neighboring cells or cells underneath pushing outward. The current cell shape matrix M_c (red ellipse) is the deformed shape of the cell observed in the tissue. (e) The anisotropic growth of the cells depends on the yielding of cell wall and mechanical stresses on the cells. The mechanical feedback inhibits growth in the higher stress direction and boosts growth in the orthogonal direction. The growth of a cell's rest shape M_c^0 under anisotropic stress with varying mechanical feedback is shown here. The highlighted ellipses (colors from the color bar) show what the rest cell shape will look like in the following time step for a given strength of mechanical feedback. The cell is initially hexagonal (gray polygon), with corresponding rest cell shape shown by black ellipse. The application of anisotropic stress (direction is shown by purple arrow) deforms the cell into its current cell shape (red polygon and red ellipse). The resulting strain from the stress is shown by blue ellipse. The mechanical feedback leads the growth of the cell's rest shape M_c^0 to be more and more orthogonal to the stress acting on the cell (ellipses, dark blue to yellow). To see this figure in color, go online.

hemicelluloses and are embedded in a matrix of pectin, are the major load-bearing component of the cell wall (12). The stiffness of the wall depends on the orientation of the fibers and is higher in the direction parallel to the orientation (13). This is crucial in promoting anisotropic cellular growth from an isotropic force arising from turgor pressure.

Cortical microtubules (CMTs), present in the cell cortex, are decisive in the deposition of new microfibrils on the cell wall because they mediate the movement of cellulose synthase complexes (14,15). The complexes move along the tracks lined by CMTs and align the cellulose microfibrils along the directions of microtubules (16,17). The orientation of CMTs itself is strongly linked with mechanical stress on the walls (4,18–20). The microtubules generally align toward the direction of maximal stress, which results in paving of cellulose microfibrils in the same direction (4,20,21). As a result, stress patterns emerging during development are a putative key actor to organize growth and shapes of tissues in plants.

Besides the elastic yielding and restructuring of the cell wall under stress, the patterns of cellular growth in plants are driven by biochemical signaling (22). In expanding walls, the cellulose microfibrils slide past each other un-

der stress in a process of polymer creeping that leads to irreversible growth (23,24). An important group of hormones that plays a major role in this growth process by loosening up the cell walls is auxin (7,25,26). Organ formation in plants at the shoot apical meristem (SAM) is preceded by accumulation of auxin (27–30). see Fig. 1. The initial outgrowth of organs from the dome-shaped SAM, called the primordia, is surrounded by localized auxin transporters that carry auxin into the incipient region (6,27). The accumulated auxin locally promotes growth in cells and initiates the formation of the primordium. During this development, disparate growth patterns emerge on the tissue. The cells at the boundary of primordia and meristem have slower and anisotropic expansion, whereas the cells in the primordia and meristem grow isotropically (31,32). The boundary also becomes saddle-shaped as the primordia grow outwards from the SAM (33,34). How these different growth patterns emerge from the initial accumulation of auxin is still puzzling.

In this work, we develop a three-dimensional vertex model for the SAM to study plant organ outgrowth. The cellular growth of the SAM is locally increased to simulate the auxin-led local initiation in higher growth rates, and the

TABLE 1 List of Symbols

Symbol	Definition
x_i, y_i	x and y coordinates for a vertex i
M_c^0	rest cell shape
M_c	current cell shape
h	primordia height
A_p	primordial area
A_T	tissue surface area
V_T	volume of tissue
A_c	area of cell
η	feedback strength
κ_p, κ_s	input growth rates for primordial and meristematic cells
κ_p^*, κ_s^*	measured growth rates for primordial and meristematic cells
γ	fluctuations strength of growth rates
r_g	growth ratio; $r_g = \kappa_p^*/\kappa_s^*$
μ	elastic stiffness
μ_b	bending stiffness
ϵ	strain on a cell
σ	stress on a cell
$\sigma_{r,o}$	stress on radial and orthonormal direction
$g_{r,o}$	measured growth of cells on radial and orthonormal direction

resulting primordial growth is studied. We find that the cellular ability to sense and respond to mechanical stresses within the tissue leads to efficient growth of a new primordium out of the SAM. We further show that mechanical feedback on cellular growth is not only responsible for emerging pattern of growth in SAM but is also involved in redistributing the stresses acting on the cells.

MATERIALS AND METHODS

Three-dimensional vertex model

Vertex models have been used to explore tissue shape in epithelial morphogenesis in a variety of model systems (2,4,35–39). A vertex model represents cells as a collection of vertices that describe their shape. They can be modeled as a polygon in two-dimensional or three-dimensional space. The cells may in addition be given a thickness by adding a height term. In our formalism, we instead use the bending stiffness of the cellular layer to represent the tissue mechanical impact of their height.

The vertices are shared between the neighboring cells, and this provides a vital advantage in modeling plant cells because they share cell walls and do not slide past each other. Each of these vertices represent a junction between cells and is subject to force balance. The movement of vertices, representing deformation of cells, arises from changes in this force balance due to processes such as cellular growth and cell division. The cells in our computational model are two-dimensional polygons but are free to move around in three-dimensional space. This allows us to investigate how individual cell growth dynamics can drive plant organ outgrowth.

Shape matrices as cell representation

To account for anisotropic cell growth, we describe the cells by a form matrix that is computed as a second moment of area matrix M (20,40). The matrix is calculated with respect to the intrinsic coordinate system for each cell, with its components given by

$$M_{xx} = \frac{1}{12} \sum_{i=1}^n a_i (y_i^2 + y_i y_{i+1} + y_{i+1}^2)$$

$$M_{xy} = M_{yx} = \frac{1}{12} \sum_{i=1}^n a_i (x_i y_{i+1} + 2x_i y_i + 2x_{i+1} y_{i+1} + x_{i+1} y_i),$$

$$M_{yy} = \frac{1}{12} \sum_{i=1}^n a_i (x_i^2 + x_i x_{i+1} + x_{i+1}^2)$$
(1)

with $a_i = (x_i y_{i+1} - x_{i+1} y_i)$, where x_i and y_i are coordinates of a vertex i measured along the intrinsic axes in the x and y direction, respectively (symbol definitions are given in Table 1). Like an elastic line under tension, there is a rest shape and a deformed shape for each cell. The rest shape is the shape that a cell c wants to acquire to reach its energy minimum and is denoted by M_c^0 . As cells reside in a tissue, they are pushed and pulled from neighboring cells. The shape that a cell is deformed into, the cell's current shape M_c , is the one that we observe in the tissue. The energy minimum for the whole tissue lies away from the individual minimum of each cells because of the intercellular coupling. This implies that all of the cells face some deformation of their rest shape in tissue's equilibrium state.

Mechanical energy of tissue

The morphology of a tissue is a result of the competition between the mechanical equilibration of the system and active biological processes inside that push it out of equilibrium. The mechanical energy for equilibration can be written as a functional with sum over costs for specific mechanical deformations. We take the functional for SAM as

$$U = U_{\text{elastic}} + U_{\text{bending}} + U_{\text{pressure}},$$
(2)

accounting for cell's elastic deformation, bending, and the plant shoot's internal pressure as discussed in detail in the following subsections. This functional is minimized to obtain the equilibrium shape of the tissue.

Strain energy for the cells

Because the cells are described as polygons embedded in three dimensions, we take a generalized relation of stresses and strains in three dimensions using the directional information of strain tensor and the Kronecker delta tensor, δ_{ij} ,

$$\sigma_{ij} = 2\mu\epsilon_{ij} + \lambda\delta_{ij} \sum_k \epsilon_{kk}.$$
(3)

The parameters λ and μ are Lamé's first and second parameters, respectively. An elastic energy density for any deformation of an isotropic material is thus written as

$$v_{\text{elastic}} = \mu \sum_{ij} \epsilon_{ij}^2 + \frac{1}{2} \lambda \left(\sum_i \epsilon_{ii} \right)^2,$$
(4)

using Eq. 3. To find the strain energy expression for the vertex model, strain and stress tensors need to be defined in terms of the shape matrices that are used to describe the cells (Eq. 1). Strain can be expressed as the difference between current shape and initial shape, written as

$$\epsilon_c = \frac{M_c - M_c^0}{\text{Tr}(M_c^0)}.$$
(5)

The stress can then be defined using Eq. 3. With these definitions, a complete expression for the elastic energy can be calculated by integrating Eq. 4 over the tissue surface to obtain

$$U_{\text{elastic}} = \mu \sum_c A_c \frac{\|M_c - M_c^0\|_2^2}{\text{tr}^2(M_c^0)} + \frac{1}{2} \lambda \sum_c A_c \frac{\text{tr}^2(M_c - M_c^0)}{\text{tr}^2(M_c^0)}, \quad (6)$$

where A_c is the area of a cell c . We set $\lambda = 0$, which is proportional to the Poisson ratio, to further simplify the elastic energy expression to

$$U_{\text{elastic}} = \mu \sum_c A_c \frac{\|M_c - M_c^0\|_2^2}{\text{tr}^2(M_c^0)}. \quad (7)$$

This simplification has no impact on the simulation results because the mechanical behavior in developing tissue can be considered stable under varying Poisson ratios (41). Our simulations prove to be qualitatively robust against variations in Poisson ratio; see [Supporting Materials and Methods](#).

The stress can then be explicitly expressed in terms of the cell shapes as

$$\sigma_c = 2\mu \frac{M_c - M_c^0}{\text{Tr}(M_c^0)}. \quad (8)$$

Bending energy of the tissue

Previous authors have noted the response of the SAM is close to a stiff shell inflated by a pressure (42). This suggests that the turgor pressure from within the tissue is sustained by either the outer layer of cells or only the outer walls of those cells. We thus consider the meristem as a single layer of stiff cells on a two-dimensional surface, free to move in three-dimensional space. For epithelial cells in a tissue, the cells are restricted first, by the walls that are perpendicular to the surface (anticlinal walls), and second, by junctions with cells around them. Any significant bend or twist away from the epithelial surface would mean a major deformation on the anticlinal walls and on cells underneath. Thus, we add a bending term to the mechanical energy that penalizes deformations of anticlinal walls. It is based on the works of Canham and Helfrich, who considered a three-dimensional soft object with an infinitely thin interface with bending resistance (43–45),

$$U_{\text{bending}} = 2\mu_b \int_S (H - H_0)^2 dA + \int_S \mu_K K dA, \quad (9)$$

$$H = \frac{1}{2}(k_1 + k_2), \quad (10)$$

$$K = k_1 k_2, \quad (11)$$

where H is the local mean curvature and K is the Gaussian curvature. k_1 and k_2 are the principal curvatures at a point on the tissue surface S . H is taken to be positive for the dome shape of the shoot tip. The Gaussian curvature K can be integrated out of the energy equation because it remains constant for a surface with fixed topology, which leaves only the first term for bending energy (46,47). Discretization of H developed by Meyers et al. is used to compute Eq. 9 for the tissue in our simulations (45,47).

Pressure inside the tissue

The cells below the surface epithelial layer of the shoot apex push outwards on the surface layer. The net force acting on the cells in the surface layer

promotes outward growth. Following previous approaches (4,35,48), we represent this outward pressure by an additive pressure term in the energy,

$$U_{\text{pressure}} = -PV_T, \quad (12)$$

where P is the pressure from underneath and V_T is the volume of the total shoot apex. Note that the contribution of internal pressure within individual cells can be subdivided into a perpendicular and an in-plane contribution. Under the assumption of equal pressure in all cells, the in-plane contribution cancels out (4); the perpendicular component has the same functional form as above and, as such, is reflected in the term as well.

Energy minimization and boundary condition

The equilibrium shape of the tissue is found by minimization of the mechanical energy Eq. 2 using the SubPlex algorithm implemented in the open source nonlinear optimization library NLOPT (49,50). During the entire simulation, the vertices at the lower boundary of the tissue are fixed in their position (Fig. 1, a–c), representing the connection of the SAM to mature and hardened cells of the shoot.

Cellular growth through deformation

Cellular growth in plants has long been regarded as a mechanical process, with yielding of the cell wall leading growth under turgor pressure. Lockhart considered the cell wall as a Bingham fluid and proposed to model a cell's growth proportional to the deformation on the cells (9). Adapting this definition for the vertex model, we write

$$\frac{dM_c^0}{dt} = \kappa(1 + \gamma)(M_c - M_c^0)_+, \quad (13)$$

where κ is the growth rate of cells, fluctuating with amplitude γ . γ represents the variation arising in the cellular growth, including the variations in turgor pressure present between the cells that might result in inhomogeneous growth. The difference of the current shape, M_c , and the rest shape, M_c^0 , i.e., the deformation on the cells, drives the growth. The operation $(\cdot)_+$ ensures that the cells do not shrink even if the cells are faced with negative deformation under compressive stresses (Eq. S2). This operation only allows positive growths led by positive deformations.

CMT-led mechanical feedback on cell wall

The anisotropic cellular expansion and growth patterning in plants depend on the anisotropic cell-wall stiffness because the forces generating growth are isotropic. The reorganization of CMT orientation led by stresses and the subsequent cellulose microfibril deposition promoting wall anisotropy can be represented by the dynamics of the rest cell shape (20,40). Given the observation that CMTs orient according to the highest stress and thus reduce growth in the direction of highest stress, we model this effect by coupling the growth rate to the cell's asymmetric stress component, the deviatoric stress $D_c = \sigma_c - 1/2 \text{Tr} \sigma_c$, thus extending the growth equation Eq. 13 to

$$\begin{aligned} \frac{dM_c^0}{dt} &= \kappa(1 + \gamma)(M_c - M_c^0) \\ &\quad - \frac{\eta}{2}(D_c(M_c - M_c^0) + (M_c - M_c^0)D_c). \end{aligned} \quad (14)$$

The feedback parameter η quantifies the rate of rest shape reorganization per unit of stress for a cell. It represents the cell wall's ability to respond to stress, and with higher η , the efficiency of reorganizing of the cell walls is higher. Increasing mechanical feedback results in growth that is more and

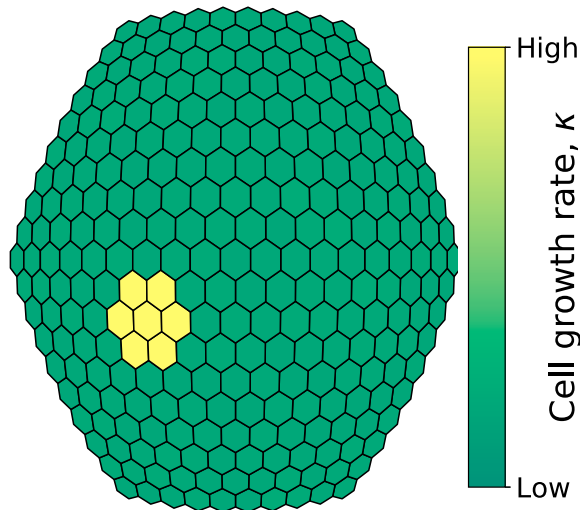


FIGURE 2 The localized accumulation of auxin causes an increased growth rate in primordium cells (yellow), top-down view on shoot tip. This is modeled by assigning higher growth rate to cells of the designated primordial region. The chosen parameters for the simulation are listed in Table S1. The system is robust under parameter changes up to two orders of magnitude for pressure and stiffness, whereas a growth ratio larger than 10 can lead to strong artifacts in cell shapes. To see this figure in color, go online.

more orthogonal to the higher stress direction, as expected from the wall strengthening in that direction (Fig. 1 e; Fig. S14). This anisotropic growth of the cells by the modulation of rest cell shape with mechanical feedback takes into account the anisotropic properties of cell walls, which are not directly included in the elastic energy density.

The reorganization of the wall stiffness in the cells from the mechanical feedback can be measured by comparing the growth of the cells to its deformation. Supporting Materials and Methods details the measure for the stiffness modulation of the cells.

Localized enhanced growth rate

The plant growth hormone auxin causes a reduction in cell-wall hemicellulose polysaccharides and an increase in pectin polymerization and viscosity, among other roles in plant biology (25,26,51,52). It initiates organ formation on the SAM by increasing the growth rate of primordial cells through loosening of the cell walls (4,7,27). Yet, the faster-growing cells in primordial region are still tightly connected to the slower-growing cells in the meristem tissue through shared cell walls (4,35,53). Thus, it is unclear how fast both primordial and meristem cells can effectively grow and how both kinds of cells deform because of the localized enhanced growth rate. To study tissue growth and deformation, we define a prepatterned localization of auxin in the SAM (Fig. 2) with an enhanced growth rate κ_f relative to the surrounding meristem tissue with κ_s as input parameters to Eq. 14. Because of the cell-cell junctions and tissue mechanics constraining the cells, the actual growth rates of cells, κ^* , is less than specified by the input parameters. The rates κ_f^* and κ_s^* are measured in simulations by fitting an exponential growth curve to the area growth of primordial and meristematic cells, respectively (Fig. S5). Ultimately, the ratio

$$r_g = \kappa_f^* / \kappa_s^* \quad (15)$$

of these two growth rates is what is governing the growth of the entire tissue. The two values (κ^* and κ) are not equal because the cellular growth is affected by tissue mechanics, cellular interactions, and mechanical feedback.

RESULTS

Growth of the SAM

Aerial organs in plants start out as primordia in the SAM, initiated by differential growth of cells. During the emergence of primordia, cells in primordia are observed to grow faster and isotropically, whereas the cells in boundary region between the primordia and the rest of the meristem have arrested growth and are highly anisotropic (32,33,54). To understand the cause of these growth patterns, the overall role of mechanics-led growth feedback, and their effect on primordium outgrowth, we developed a three-dimensional vertex model to simulate the growth of SAM.

We take the SAM as a hemispherical surface composed of homogeneous hexagonal cells that have been relaxed under the chosen simulation parameters. With a uniform cellular growth rate κ (see Eq. 13) for all cells, the tissue expands without significant morphological changes on the surface (Fig. 3, a and b). The growth of the SAM is driven by the deformation of the surface cells due to the volume pressure from the tissue underneath.

Plant organ outgrowth on the SAM is observed when the tissue is prepatterned with a localized higher growth rate, corresponding to localized auxin accumulation in primordial cells (Fig. 2). The faster-growing region bulges out from the tissue surface, as shown in Figs. 3, c and d and 4. We quantify this outgrowth of the primordium by measuring the height of the bulge as

$$h = \|\vec{v}_{\text{top}} - \vec{v}_{\text{boundary}}\|, \quad (16)$$

where $\vec{v}_{\text{boundary}}$ is the average position of the vertices at the boundary of the primordial region and \vec{v}_{top} is the position vector to the centroid of the cell at the top of the primordium, as shown in Fig. S1.

We analyze the outgrowth height as a function of tissue surface area to facilitate a comparison independent of the chosen intrinsic cell growth rates. The total simulation time and cellular growth over one time step can differ significantly depending on the choice of growth rates. However, because all of the dynamics in biology follow a robust time-scale for the growth, we use the growth of the tissue surface area as an indicator for time to compare simulated tissues under different sets of parameters.

In the following sections, we examine the simulation results of organ outgrowth to investigate the role of tissue mechanics during primordial growth.

Differential growth leads to primordial outgrowth

The faster growth rates of primordial cells push against the SAM surface, leading to the bulging out of the tissue. Here, the ratio of growth rates r_g (Eq. 15) dictates bulge formation. Increasing r_g leads to higher outgrowth (see Fig. 5 b), going hand in hand with stronger growth of primordial cells and the formation of bigger-sized bulges (Fig. 5 a). Changing

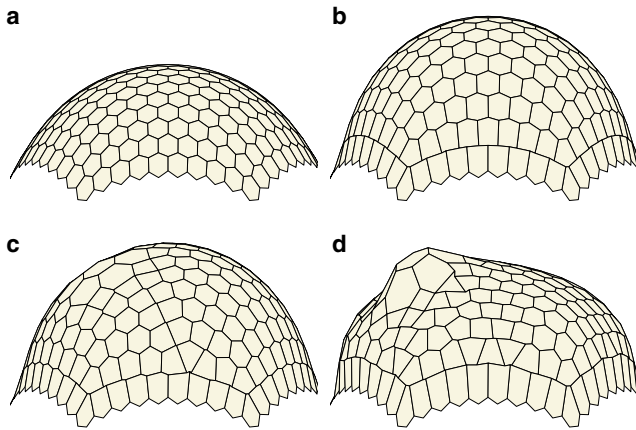


FIGURE 3 Growth of the SAM under varying growth conditions. (a) The initial shape of a tissue used for all growth simulation with surface area $A_T = 665$. (b)–(d) are the resulting shapes after tissue has grown to $A_T = 850$. (b) Growth with uniform growth rate $\kappa = 0.5$. (c) Growth with growth ratio $r_g = 4.8$ and no mechanical feedback $\eta = 0$. (d) Growth, also with growth ratio $r_g = 4.8$ but high mechanical feedback $\eta = 8$. To see this figure in color, go online.

both the primordial and meristematic growth rates while keeping the growth ratio constant has no effect on the height dynamics (Fig. S6). To further explore the emergence of primordia, we next introduce a mechanical feedback on cellular growth to tissue-wide mechanical stresses and study its impact on outgrowth dynamics.

Active mechanical response from cells drives outgrowth

Mechanical stresses in tissue are propagated among cells through shared cell walls. As a response to the mechanical stresses acting on them, the cells actively remodel cell walls. This microtubule-led reorganization of walls and cellular growth is considered to be vital for robust morphogenesis. We model this feedback by implementing a stress-dependent term in the growth equation that accounts for active strengthening of walls in higher stress direction (Eq. 14).

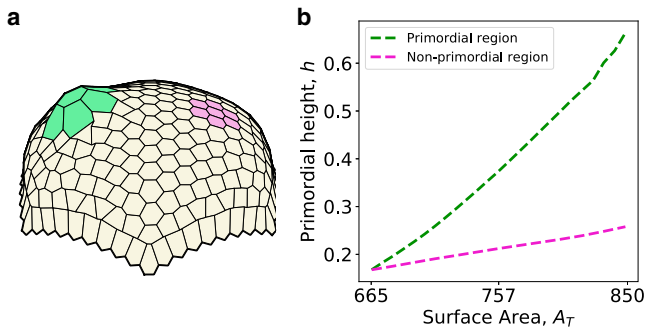


FIGURE 4 Comparison of tissue height in primordial and nonprimordial region shows the presences of significant outgrowth in primordial region. (a) Regions of primordia (green) and nonprimordia (magenta) are shown on the tissue. (b) Increase in height of primordial and nonprimordial region. To see this figure in color, go online.

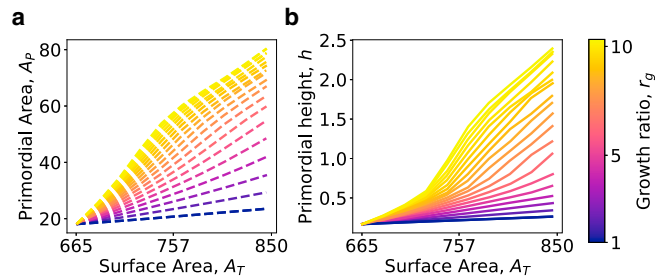


FIGURE 5 Higher growth ratio leads to higher primordial growth. The growth rate for meristem (κ_s) is kept constant while the primordial growth rate (κ_f) is increased for larger growth ratio. (a) The primordium grows larger with increasing growth ratio. (b) The primordium bulges out further because of the increase in its size, as seen with higher primordial height on greater growth ratio. To see this figure in color, go online.

We find that the ability of cells to sense stresses and react accordingly is vital for organ outgrowth on the meristem. By modulating the mechanical feedback of a tissue, we observe that the outgrowth is higher when cellular response to mechanics is enhanced (Fig. 6 b). This observation in our simulation is in agreement with previous experimental observations (4,55).

Note that contrary to the dynamics for an increasing growth ratio, increasing mechanical feedback only promotes outgrowth height while leaving the primordial tissue area almost unchanged (Figs. 5 a and 6 a). This indicates that mechanical feedback promotes organ outgrowth by a different mechanism than effective increase in growth rate. Notably, growth rates in cells of primordial and meristematic regions are unaffected by mechanical feedback, keeping the growth ratio fixed. Thus, it is the more puzzling that the reorganization of growth led by mechanical feedback is able to bulge out the primordium more efficiently with increasing feedback. A little bit of insight can already be gained from the simulation snapshots in Fig. 3, c and d, in which tissues of the same overall area with and without feedback are compared. The growth is directed outwards for the primordium with mechanical feedback, leading to

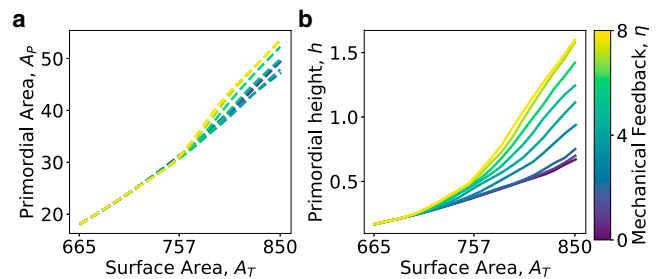


FIGURE 6 Increasing mechanical feedback of cells to tissue-wide mechanical stresses results in efficient primordial growth. Here, a tissue with growth ratio $r_g = 4.8$ is grown for varying mechanical feedback. (a) The overall areal growth of the primordium is relatively unchanged with changing mechanical feedback. (b) The height of the primordium increases significantly with higher mechanical feedback. To see this figure in color, go online.

a clear bulging (Fig. 3 *d*), whereas the primordial cells without feedback grow predominantly within the meristem surface but are not able to bulge outwards (Fig. 3 *c*).

Diverging stresses reorganize growth in boundary cells

We next investigated how growth is reorganized within the tissue by the mechanical feedback and how it can lead to greater height growth in primordia. The differential growth rates between the primordium and meristem reshape stress patterns on the SAM, which are used by cells through mechanical feedback to reorganize their growth. Mapping out the radial and orthoradial stresses on the cells at the boundary of the primordium (Fig. S2), we find that the stress distribution in boundary cells becomes more and more anisotropic during growth with increasing mechanical feedback (Fig. 7 *a*). The orthoradial stress σ_o (circumferential direction to the primordium) in boundary cells remains high throughout the primordial growth, whereas the radial stress σ_r (direction toward the tip of the primordium) declines.

As expected from the mechanical feedback, the growth of the boundary cells also exhibits distinct anisotropic patterns (Fig. 7 *b*). In the absence of feedback, both orthoradial and radial growth stay at a more or less constant high level, with orthoradial growth being about twice as large as radial

growth. Mechanical feedback drives both orthoradial and radial growth to plummet over time to smaller and smaller growth, eventually ceasing growth entirely at high mechanical feedback. The cessation of growth of the boundary cells is clearly visible when plotting the total area of boundary cells during growth; see Fig. 7 *c*. Further, the relative stiffness reorganization also shows the trend of growing anisotropic wall properties arising from the mechanical feedback (Figs. S7 and S8). The stiffness is enhanced in the orthoradial direction and is lowered in the radial direction. Importantly, this enhancement is observed to be significantly boosted with the mechanical feedback. These trends of growth and mechanical patterning remained intact with the introduction of a Poisson ratio on the system (Fig. S15).

Increasing mechanical feedback not only leads to the slower growth and stiffening of the boundary region but also to its compression (Fig. 7 *c*) because of the increasing stresses from neighboring cells (note negative stresses arising in Fig. 7 *a*). In addition, the shape of the boundary is also seen to be dependent on the mechanical regulation of cell growth. The Gaussian curvature, indicating the saddle shape of the boundary, is observed to be increasingly negative with feedback (Fig. S12 *c*).

We infer from these observations that the reorganization of growth and stiffness in primordium boundary cells due to mechanical feedback to the arising stresses is the vital mechanism behind the efficient outgrowth of organ primordium.

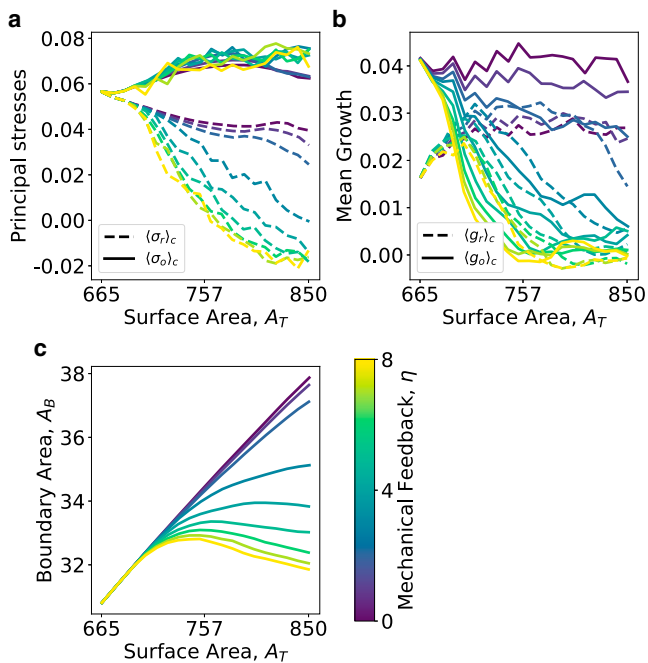


FIGURE 7 Pattern of stresses and growth in boundary cells undergo significant modification by mechanical feedback. Here, $\langle \cdot \rangle_c$ represents an average over the cells in the boundary of primordium. (a) Stresses in radial (σ_r) and orthoradial (σ_o) directions diverge during growth more and more with increasing feedback. (b) Growth rates of boundary cells decay with feedback. (c) The boundary cells not only cease in growth but are also compressed by primordium and meristem cells. To see this figure in color, go online.

Mechanical feedback modulates the height growth rate

To link the relation of generated stress pattern and growth reorganization caused by mechanical feedback, we examine the rate of height growth in the primordium with respect to the growth of the tissue surface as a function of anisotropy in stresses on boundary cells (Fig. 8). The stress anisotropy

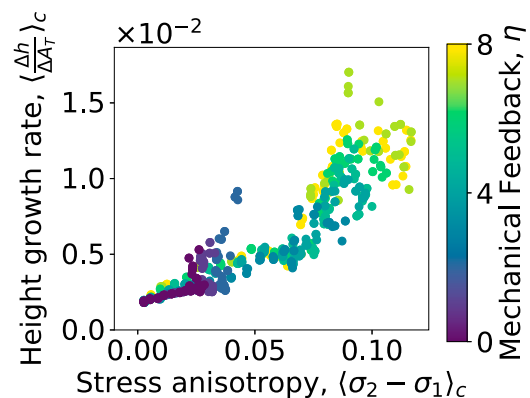


FIGURE 8 Rate of primordial height growth is boosted significantly by mechanical feedback. With higher mechanical feedback, both the rate of height growth and the stress anisotropy of cells on the primordial boundary increase. By this two-way reinforcement, mechanics is able to guide efficient primordium outgrowth on the SAM. To see this figure in color, go online.

was defined as the difference between the two principal stresses acting on the cells. We observe that along with the boost in the height growth rate, which results directly from cellular growth reorganization, mechanical feedback generates greater stress anisotropy in boundary cells. The averaged differences in principal stresses increase with higher mechanical feedback. This helps to amplify the growth heterogeneity in the tissue and establishes the large-scale stress pattern that promotes efficient organ outgrowth. Without the mechanical feedback, both height growth rate and stress anisotropy are low; see Fig. 8. Only the stress anisotropy in boundary cells arising from mechanical feedback, also seen by diverging stress in Fig. 7 *a*, allows the growth reorganization in cells that results in a strong growth in primordium height.

DISCUSSION

We developed a three-dimensional vertex model for plant development to understand how a primordium, as a precursor of aerial organs, can grow out on the SAM given the tight connections of cells via plant cell walls. After the initialization by biochemically triggered local wall softening, resulting in higher growth rate in the primordial region, we quantify outgrowth dynamics by organ height above tissue level. Taking into account mechanical feedback mediated by CMTs, which reinforce cell walls in the direction of higher mechanical stress and promotion of growth in the orthogonal direction, we observe higher and more efficient primordium outgrowth.

The cell-based approach of the vertex model for plant tissue developed here ensures the direct coupling of growth of the cells in different directions (expressed with Eq. 14). This removes the requirement of additional equations and parameters for modeling the mechanical feedback in growth. The artifacts displayed during later stages of simulations on the wall shapes of the cells (visible in Fig. 4, *b–d*, with shrinking walls in some boundary cells) has little impact on the cell-shape computation. The shape matrices defined by the second moment of the area depend on areal distribution of the cells. They are not distorted with simple artifacts such as shrinking of walls (Figs. S16 and S17). This is a major advantage for using a cell-based vertex model rather than the wall-based one, which can be highly susceptible to shape distortions. The cell-based shape method also facilitates direct comparison of simulation results with experimental data, which are abundant with mapped-out differences in growth at cellular level (56). The experimental data at the wall level are still scarce for comparison.

Keeping in mind the robust growth rates in plant tissues, we used the surface area of the meristem as a proxy for age to compare the morphology of the tissue across different parameters. Higher growth rates in the primordial region with respect to the surrounding meristematic tissue were sufficient to trigger organ outgrowth (Fig. 5 *b*). We found that

the absolute values of primordial and meristematic growth rates are irrelevant because the dynamics of primordium formation is dictated by the ratio of growth rates between the faster-growing primordial cells to the slower-growing meristematic cells (Fig. S6). However, with mechanical feedback of cell growth on tissue-wide mechanical stresses, organ shaping is more efficient.

Although mechanical feedback does not strongly impact the overall growth of a primordium in area, it directly controls the height of the primordium (Fig. 6). Mechanical feedback can account for the same height with half the growth rate as seen in the following example: the primordia of tissue with growth ratio $r_g = 4.8$ and mechanical feedback of $\eta = 8$ was able to grow to the same height ($h = 1.6$ at $A_T = 850$) as the tissue with twice the growth ratio $r_g = 9.6$ without feedback. Thus, utilizing the CMT-mediated mechanical feedback, plants are able to push out organs from the SAM in a faster and more efficient manner.

We found that the surprising increase in organ height is due to the reorganization of growth and stress on the cells at the boundary of primordia (Fig. 7, *a–c*). Boundary cells are under considerable anisotropic stress, and this stress anisotropy is further enhanced by mechanical feedback (Fig. 7 *a*). Larger stresses along the boundary of the growing primordia generated by the mechanical feedback (Fig. S11) can also account for the emergence of circumferential alignment of CMTs in the boundary region, as has been noted in the experiments (4). This implicates the CMT alignment, which follows higher stress, with the reorganization of growth by mechanics in plant cells.

The mechanical feedback is observed to slow down boundary cell growth and even cease growth for high feedback (Fig. 7 *b*). In addition, the stiffness of walls in the boundary cells are found to be significantly strengthened in the orthoradial direction and loosened in the radial direction by mechanical feedback (Fig. S7 as compared to Fig. S8). Because the primordial area is unaffected by the feedback (Fig. 6 *a*), the key role of boundary cells is to act as a stiff and slow-growing ring on the tissue surface that pushes out the primordium. An earlier study has noted the effectiveness of a stiff ring-like boundary in the development of primordia (35). Now, we are able to accredit the emergence of such larger-scale patterns in the tissue without a central organizer to the mechanical feedback in the cellular growth.

The boundary region is even compressed because of the strong stresses from the meristem and primordium in the high-feedback regime (Fig. 7 *c*). The decrease in the area of boundary cells is due to the compressive stresses arising from the primordial development (negative radial stresses seen in Fig. 7 *b*). Because the cells are restricted from shrinking from their rest shape (Eq. 13), this compression of cells is purely elastic. Similar compression of the boundary cells has been noted *in vivo* in cells surrounding a growing primordium (33). With the introduction of a

Poisson ratio to the system ($\nu = 0.375$), we found that the boundary compression could be reduced (Fig. S15 c), but the boundary growth still halted thereby supporting higher primordial outgrowth (Fig. S15, a–d). We thus identified an entirely different mechanism that effectively acts analogously to contractile-ring-like dynamics also known to cause shape transformations in animal epithelial tissue (37).

Our results also indicate that the saddle shape of the boundary region and the anisotropic shapes of the boundary cells are dependent on the mechanical feedback. Larger negative values of Gaussian curvature can be observed for the case with high mechanical feedback, whereas for no or low feedback, the boundary has, on average, positive Gaussian curvature (Fig. S12). This suggests that the saddle-like boundary with negative curvatures, as observed in experiments (33,34), can emerge from the growth patterns created by mechanical feedback. Further, the shape of the cells themselves in the boundary was found to be progressively anisotropic with mechanical feedback (Fig. S13), again suggesting that the tissue-wide morphology of the cells can be guided by the reorganized mechanics of the tissue by the stress-based feedback.

Although a decrease in circumferential strain along with the promotion of axial strains in primordium boundary cells has been suggested to promote primordium outgrowth (55), we show here how such growth dynamics can self-organize because of mechanical feedback. We can therefore finally explain experimental observations of very low or no growth and even compression of cells in the boundary region (32,33,48,54). The emerging mechanical patterning can also be suspected as the cause for the separation of meristem and primordium because it mechanically establishes a distinct boundary region on the SAM.

Correlating primordial height growth rate and boundary cell stress anisotropy for different values of mechanical feedback (Fig. 8), we observe a clear connection substantiating that boundary cell stress anisotropy increase, proportional to mechanical feedback, is driving primordium outgrowth. Interestingly, for high mechanical feedback, stress anisotropy and height growth rate saturate. This suggests that the gain in primordial growth flattens out in the high-feedback regime, and there could be an optimal level of mechanical feedback for efficient growth in plants, clarifying previous model observations (40).

Future investigations can be targeted to explore the influence of other biological processes, such as cell divisions, on the growth of the primordia. Preliminary results from our simulations show the impact of mechanical feedback to remain intact with cell division (Fig. S9). However, there are strong patterns of cell division observed during primordial development. Primordial cells are known to exhibit higher rates of divisions compared to the meristematic cells (57), and the divisions in boundary cells have been suggested to orient following the stress (48). The study of such divisions in primordial growth can elucidate the intricate role of divisions

in morphological development and also help in understanding the preferential direction and timing of the cells for division.

The expansion of the model from two-dimensional surface to a full description in three dimensions can also be considered for future work. Modulating the bending stiffness for the cells, which represents the stiffness of the anticlinal walls, does show an impact on the magnitude of primordial growth (Fig. S10). A feedback of stresses with stiffness in the anticlinal direction can also be examined to further understand the overall regulation of plant cell growth by tissue mechanics.

With these results taken together, our key insight is that mechanical feedback reorganizes cell growth by two distinct mechanisms. First, feedback directly influences cell growth by modulation of wall properties. Second, feedback changes the stress patterns on cells, thereby self-amplifying and propagating growth anisotropies that then indirectly influence cell growth again. This twofold mechanism allows plant tissue to initiate organ outgrowth efficiently by modifying their growth pattern through stress feedback rather than amplifying growth rates at the expense of cell material.

SUPPORTING MATERIAL

Supporting Material can be found online at <https://doi.org/10.1016/j.bpj.2019.10.019>.

AUTHOR CONTRIBUTIONS

J.K., J.-D.J., and K.A. designed research. J.K. performed the research. J.K., J.-D.J., and K.A. wrote the article.

ACKNOWLEDGMENTS

This work was in part supported by the Max Planck Society and the Deutsche Forschungsgemeinschaft via grants SFB-937/A19 and DFG-FOR 2581.

REFERENCES

- Hong, L., M. Dumond, ..., A. H. Roeder. 2016. Variable cell growth yields reproducible organdevlopment through spatiotemporal averaging. *Dev. Cell.* 38:15–32.
- Farhadifar, R., J. C. Röper, ..., F. Jülicher. 2007. The influence of cell mechanics, cell-cell interactions, and proliferation on epithelial packing. *Curr. Biol.* 17:2095–2104.
- Osterfield, M., C. A. Berg, and S. Y. Shvartsman. 2017. Epithelial patterning, morphogenesis, and evolution: *Drosophila* eggshell as a model. *Dev. Cell.* 41:337–348.
- Hamant, O., M. G. Heisler, ..., J. Traas. 2008. Developmental patterning by mechanical signals in *Arabidopsis*. *Science.* 322:1650–1655.
- Baskin, T. I. 2005. Anisotropic expansion of the plant cell wall. *Annu. Rev. Cell Dev. Biol.* 21:203–222.
- Heisler, M. G., O. Hamant, ..., E. M. Meyerowitz. 2010. Alignment between PIN1 polarity and microtubule orientation in the shoot apical meristem reveals a tight coupling between morphogenesis and auxin transport. *PLoS Biol.* 8:e1000516.
- Nakayama, N., R. S. Smith, ..., C. Kuhlemeier. 2012. Mechanical regulation of auxin-mediated growth. *Curr. Biol.* 22:1468–1476.

8. Long, Y., and A. Boudaoud. 2019. Emergence of robust patterns from local rules during plant development. *Curr. Opin. Plant Biol.* 47:127–137.
9. Lockhart, J. A. 1965. An analysis of irreversible plant cell elongation. *J. Theor. Biol.* 8:264–275.
10. Ray, P. M., P. B. Green, and R. Cleland. 1972. Role of turgor in plant cell growth. *Nature.* 239:163–164.
11. Green, P. B. 1962. Mechanism for plant cellular morphogenesis. *Science.* 138:1404–1405.
12. Mirabet, V., P. Das, ..., O. Hamant. 2011. The role of mechanical forces in plant morphogenesis. *Annu. Rev. Plant Biol.* 62:365–385.
13. Kerstens, S., W. F. Decraemer, and J. P. Verbelen. 2001. Cell walls at the plant surface behave mechanically like fiber-reinforced composite materials. *Plant Physiol.* 127:381–385.
14. Ledbetter, M. C., and K. R. Porter. 1963. A "microtubule" in plant cell fine structure. *J. Cell Biol.* 19:239–250.
15. Heath, I. B. 1974. A unified hypothesis for the role of membrane bound enzyme complexes and microtubules in plant cell wall synthesis. *J. Theor. Biol.* 48:445–449.
16. Paredez, A. R., C. R. Somerville, and D. W. Ehrhardt. 2006. Visualization of cellulose synthase demonstrates functional association with microtubules. *Science.* 312:1491–1495.
17. Somerville, C. 2006. Cellulose synthesis in higher plants. *Annu. Rev. Cell Dev. Biol.* 22:53–78.
18. Wymer, C. L., S. A. Wymer, ..., R. J. Cyr. 1996. Plant cell growth responds to external forces and the response requires intact microtubules. *Plant Physiol.* 110:425–430.
19. Cleary, A. L., and A. R. Hardham. 1993. Pressure induced reorientation of cortical microtubules in epidermal cells of *Lolium rigidum* leaves. *Plant Cell Physiol.* 34:1003–1008.
20. Uyttewaal, M., A. Burian, ..., O. Hamant. 2012. Mechanical stress acts via katanin to amplify differences in growth rate between adjacent cells in *Arabidopsis*. *Cell.* 149:439–451.
21. Landrein, B., and O. Hamant. 2013. How mechanical stress controls microtubule behavior and morphogenesis in plants: history, experiments and revisited theories. *Plant J.* 75:324–338.
22. Cosgrove, D. J. 2016. Plant cell wall extensibility: connecting plant cell growth with cell wall structure, mechanics, and the action of wall-modifying enzymes. *J. Exp. Bot.* 67:463–476.
23. Marga, F., M. Grandbois, ..., T. I. Baskin. 2005. Cell wall extension results in the coordinate separation of parallel microfibrils: evidence from scanning electron microscopy and atomic force microscopy. *Plant J.* 43:181–190.
24. Cosgrove, D. J. 2005. Growth of the plant cell wall. *Nat. Rev. Mol. Cell Biol.* 6:850–861.
25. Ray, P. M. 1962. Cell wall synthesis and cell elongation in oat coleoptile tissue. *Am. J. Bot.* 49:928–939.
26. Majda, M., and S. Robert. 2018. The role of auxin in cell wall expansion. *Int. J. Mol. Sci.* 19:E951.
27. Reinhardt, D., E. R. Pesce, ..., C. Kuhlemeier. 2003. Regulation of phyllotaxis by polar auxin transport. *Nature.* 426:255–260.
28. Benková, E., M. Michniewicz, ..., J. Friml. 2003. Local, efflux-dependent auxin gradients as a common module for plant organ formation. *Cell.* 115:591–602.
29. Heisler, M. G., C. Ohno, ..., E. M. Meyerowitz. 2005. Patterns of auxin transport and gene expression during primordium development revealed by live imaging of the *Arabidopsis* inflorescence meristem. *Curr. Biol.* 15:1899–1911.
30. Kwiatkowska, D. 2008. Flowering and apical meristem growth dynamics. *J. Exp. Bot.* 59:187–201.
31. Kwiatkowska, D. 2004. Surface growth at the reproductive shoot apex of *Arabidopsis thaliana* pin-formed 1 and wild type. *J. Exp. Bot.* 55:1021–1032.
32. Aida, M., and M. Tasaka. 2006. Morphogenesis and patterning at the organ boundaries in the higher plant shoot apex. *Plant Mol. Biol.* 60:915–928.
33. Kwiatkowska, D., and J. Dumais. 2003. Growth and morphogenesis at the vegetative shoot apex of *Anagallis arvensis* L. *J. Exp. Bot.* 54:1585–1595.
34. Dumais, J., and D. Kwiatkowska. 2002. Analysis of surface growth in shoot apices. *Plant J.* 31:229–241.
35. Boudon, F., J. Chopard, ..., C. Godin. 2015. A computational framework for 3D mechanical modeling of plant morphogenesis with cellular resolution. *PLoS Comput. Biol.* 11:e1003950.
36. Osterfield, M., X. Du, ..., S. Y. Shvartsman. 2013. Three-dimensional epithelial morphogenesis in the developing *Drosophila* egg. *Dev. Cell.* 24:400–410.
37. Misra, M., B. Audoly, ..., S. Y. Shvartsman. 2016. Shape transformations of epithelial shells. *Biophys. J.* 110:1670–1678.
38. Alt, S., P. Ganguly, and G. Salbreux. 2017. Vertex models: from cell mechanics to tissue morphogenesis. *Philos. Trans. R. Soc. Lond. B Biol. Sci.* 372:20150520.
39. Fozard, J. A., M. Lucas, ..., O. E. Jensen. 2013. Vertex-element models for anisotropic growth of elongated plant organs. *Front. Plant Sci.* 4:233.
40. Alim, K., O. Hamant, and A. Boudaoud. 2012. Regulatory role of cell division rules on tissue growth heterogeneity. *Front. Plant Sci.* 3:174.
41. Bozorg, B., P. Krupinski, and H. Jönsson. 2014. Stress and strain provide positional and directional cues in development. *PLoS Comput. Biol.* 10:e1003410.
42. Beauzamy, L., M. Louveaux, ..., A. Boudaoud. 2015. Mechanically, the shoot apical meristem of *Arabidopsis* behaves like a shell inflated by a pressure of about 1 MPa. *Front. Plant Sci.* 6:1038.
43. Canham, P. B. 1970. The minimum energy of bending as a possible explanation of the biconcave shape of the human red blood cell. *J. Theor. Biol.* 26:61–81.
44. Helfrich, W. 1973. Elastic properties of lipid bilayers: theory and possible experiments. *Z. Naturforsch. C.* 28:693–703.
45. Guckenberger, A., M. P. Schraml, ..., S. Gekle. 2016. On the bending algorithms for soft objects in flows. *Comput. Phys. Commun.* 207:1–23.
46. Gompper, G., and D. M. Kroll. 1996. Random surface discretizations and the renormalization of the bending rigidity. *J. Phys. I.* 6:1305–1320.
47. Meyer, M., M. Desbrun, ..., A. H. Barr. 2003. Discrete differential-geometry operators for triangulated 2-manifolds. In *Visualization and Mathematics III*. H. C. Hege and K. Polthier, eds. Springer, pp. 35–57.
48. Louveaux, M., J. D. Julien, ..., O. Hamant. 2016. Cell division plane orientation based on tensile stress in *Arabidopsis thaliana*. *Proc. Natl. Acad. Sci. USA.* 113:E4294–E4303.
49. Rowan, T. H. 1990. Functional stability analysis of numerical algorithms. PhD thesis. University of Texas at Austin.
50. Johnson, S. G. The NLOpt nonlinear-optimization package. <http://ab-initio.mit.edu/nlopt>.
51. Nishitani, K., and Y. Masuda. 1981. Auxin-induced changes in the cell wall structure: changes in the sugar compositions, intrinsic viscosity and molecular weight distributions of matrix polysaccharides of the epicotyl cell wall of *Vigna angularis*. *Physiol. Plant.* 52:482–494.
52. Perrot-Rechenmann, C. 2010. Cellular responses to auxin: division versus expansion. *Cold Spring Harb. Perspect. Biol.* 2:a001446.
53. Rebocho, A. B., P. Southam, ..., E. Coen. 2017. Generation of shape complexity through tissue conflict resolution. *eLife.* 6:e20156.
54. Reddy, G. V., M. G. Heisler, ..., E. M. Meyerowitz. 2004. Real-time lineage analysis reveals oriented cell divisions associated with morphogenesis at the shoot apex of *Arabidopsis thaliana*. *Development.* 131:4225–4237.
55. Oliveri, H., J. Traas, ..., O. Ali. 2019. Regulation of plant cell wall stiffness by mechanical stress: a mesoscale physical model. *J. Math. Biol.* 78:625–653, Published online September 12, 2018.
56. Kwiatkowska, D. 2006. Flower primordium formation at the *Arabidopsis* shoot apex: quantitative analysis of surface geometry and growth. *J. Exp. Bot.* 57:571–580.
57. Laufs, P., O. Grandjean, ..., J. Traas. 1998. Cellular parameters of the shoot apical meristem in *Arabidopsis*. *Plant Cell.* 10:1375–1390.